Probabilistic Engineering Mechanics 74 (2023) 103512

Contents lists available at ScienceDirect

Probabilistic Engineering Mechanics

journal homepage: www.elsevier.com/locate/probengmech

Bayesian inference of pit corrosion in prestressing strands using Markov Chain Monte Carlo method

Jaebeom Lee [a], Chi-Ho Jeon [b], Chang-Su Shim [b], Young-Joo Lee [c,*]

[a] Intelligent Wave Engineering Team, Korea Research Institute of Standards and Science (KRISS), Daejeon 34113, Republic of Korea
[b] Department of Civil and Environmental Engineering, Chung-Ang University, Seoul 06974, Republic of Korea
[c] Department of Urban and Environmental Engineering, Ulsan National Institute of Science and Technology (UNIST), Ulsan 44919, Republic of Korea

ARTICLE INFO

Keywords:
Corroded strand
Pit corrosion
Prestressed concrete bridge
Inverse analysis
Bayesian approach
Markov chain Monte Carlo (MCMC)

ABSTRACT

Corrosion monitoring has been widely studied to maintain the structural capacity of bridges through direct visual and nondestructive inspections or indirect inverse analysis-based methods. This study proposes a Bayesian inference method for inferring pit corrosion in the prestressing strands of prestressed concrete (PSC) bridges, which is an indirect method for corrosion monitoring. First, the probabilistic relationship between the mechanical properties of the strands and the amount of pit corrosion was defined using Bayes' rule. Subsequently, a Markov chain Monte Carlo method was introduced to infer the posterior probability, which is a conditional probability distribution of the amount of corrosion given a certain mechanical property. Based on the inference results, probabilistic bounds for the amount of corrosion were derived. The proposed method was applied to two examples: (a) probabilistic corrosion inference of strands based on the tensile test results, and (b) probabilistic corrosion inference of embedded strands in PSC girders based on the bending test results. The inference results demonstrated the applicability of the proposed method.

1. Introduction

Steel strands have been widely adopted as important structural components in prestressed concrete (PSC) bridges owing to their high tensile strength. To maintain the performance of PSC bridges, the strand strength must be monitored and managed. Several studies have focused on detecting corrosion which reduces the bearing capacity of girders [1]. Visual inspection has been commonly used to monitor the condition of structural components by directly observing cracks or pit corrosion. To overcome the limitations of visual inspection methods, such as the possible intervention of the inspector's subjectivity, various nondestructive techniques have been developed, including magnetic flux leakage [2], mechanical wave propagation [3,4], electromagnetic wave propagation [5,6], and electrochemical methods [7].

Indirect corrosion detection methods have also been investigated. In such methods, computer simulation models that explain the relationship between structural conditions (e.g., corrosion) and structural responses (e.g., load–deflection curves) are constructed. These simulation models are then used to inversely estimate the structural conditions (i.e., model inputs) for specific structural response data (i.e., model outputs), which is referred to as inverse analysis [8]. Yao et al. [9] proposed a damage detection method based on a verified and validated mathematical model of structures. Diaz et al. [10] proposed a method for detecting the corrosion conditions of a frigate for a specific electric sensor dataset. Similarly, Xin et al. [11] conducted an inverse analysis to detect pipe corrosion. Sousa and Gettu [12] proposed an analysis method to determine the tensile stress–crack opening curve of concrete, and Yan et al. [13] studied an optimization problem to identify corrosion in buried pipeline walls. Minagawa et al. [14] presented an inverse analysis method to detect corrosion in concrete structures, including multilayered rebars. Fonna et al. [15] studied rebar corrosion detection by integrating electrical sensor data.

These inverse analyses have recently been introduced from a probabilistic perspective. Sepahvand and Marburg [8] presented an efficient inverse stochastic method to identify uncertain elastic parameters using experimental modal data. Honzo et al. [16] proposed a Bayesian method to estimate the statistical properties of soil by considering both observational data and prior subjective information. Tada et al. [17] proposed an inverse analysis method to probabilistically predict cracks in steel plates. Fairebairn et al. [18] introduced a Monte Carlo method and deep learning model to determine the probabilistic parameters of concrete. Xu et al. [19] proposed a Bayesian method to estimate the uncertain

* Corresponding author.
E-mail addresses: jblee@kriss.re.kr (J. Lee), chihobeer@cau.ac.kr (C.-H. Jeon), csshim@cau.ac.kr (C.-S. Shim), ylee@unist.ac.kr (Y.-J. Lee).

https://doi.org/10.1016/j.probengmech.2023.103512
Received 8 January 2023; Received in revised form 12 August 2023; Accepted 14 August 2023
Available online 18 August 2023
0266-8920/© 2023 The Author(s). Published by Elsevier Ltd. This is an open access article under the CC BY-NC-ND license (http://creativecommons.org/licenses/by-nc-nd/4.0/).

parameters of carbon dioxide in air. Tsompanakis et al. [20] performed an inverse analysis to identify the input parameters for seismic analysis from a probabilistic perspective. Wang et al. [21] presented a probabilistic inverse analysis method to estimate geotechnical strength parameters, which are crucial factors for landslides. Chiachio et al. [22] proposed a Bayesian framework to predict fatigue damage using the Metropolis–Hasting (MH) algorithm. Nagel and Sudret [23] presented a probabilistic framework to infer the unknown statistical properties of the elastic modulus of civil structures. Zhao et al. [24] estimated the statistical information of geomechanical parameters such as the elastic modulus of the soil. Davidson and Waas [25] introduced a kriging and support vector machine for the probabilistic defect analysis of fiber-reinforced composites. Adeli et al. [26] compared various Bayesian methods to identify material properties of structures. Imam et al. [27] introduced a Bayesian method to investigate the compressive strength of concrete.

However, indirect methods have rarely been applied to estimate the corrosion in the prestressing strands of PSC bridges, although various computer simulation models have been developed. Cerit et al. [28] proposed a simplified finite element (FE) model to determine the mechanical properties of prestressing strands with pit corrosion. Castel et al. [29] developed an analysis model for corroded, unbonded, and post-tensioned beams, and discussed the reduction in ductility. Li et al. [30] estimated the effects of pit corrosion on the fatigue life of prestressing strands. Lee et al. [31] proposed a machine learning-based probabilistic prediction method to determine the mechanical characteristics of corroded strands by considering the pit corrosion. These studies suggest a relationship between structural conditions (e.g., corrosion) and structural responses (e.g., ultimate load and displacement). Thus, we aim to develop an inverse analysis method to infer the corrosion in prestressing strands using structural response data. This study utilizes the probabilistic model proposed by Lee et al. [31], which estimated the statistical properties of the ultimate load of steel strands for a given amount of corrosion. By introducing this as a likelihood, the probabilistic range of corrosion for a given ultimate load can be inferred from a Bayesian perspective. This method can be used to estimate the corrosion in internal tendons, which are difficult to obtain by direct corrosion measurements. A probabilistic estimate of the potential amount of corrosion is provided for the specific mechanical properties of prestressing strands.

2. Bayesian inference of pit corrosion in prestressing strands

This study proposes a new method to infer the pit corrosion in prestressing strands based on Bayes' rule [32], which establishes a relationship between two conditional probability distributions for two variables x and y as $p(x|y)$ and $p(y|x)$.

$$p(x|y) = \frac{p(y|x)p(x)}{p(y)} = \frac{p(y|x)p(x)}{\int p(y|x)p(x)dx} \tag{1}$$

where $p(x)$, $p(y|x)$, and $p(x|y)$ represent the prior probability, likelihood, and posterior probability, respectively. In several problems, estimating the integral term in the denominator requires a complex process. Thus, the proportional relationship can be introduced as follows:

$$p(x|y) \propto p(y|x)p(x) \tag{2}$$

Bayes' rule can be utilized to represent the relationship between the pit corrosion in prestressing strands and ultimate load (F_u), where the pit corrosion is represented by the sectional area at the most corroded section along with the strands (A).

$$p(A|F_u) \propto p(F_u|A)p(A) \tag{3}$$

where $p(A|F_u)$ denotes the conditional probability of the sectional area for a specific ultimate load; $p(F_u|A)$ is the likelihood of observing the ultimate load when a specific sectional area is provided; and $p(A)$ represents the prior estimate of the probability of the sectional area at the most corroded section. Eq. (3) indicates that the probability of observing the sectional area with the ultimate load can be inferred from $p(F_u|A)$ and $p(A)$. First, if A is specified, then it can be considered in terms of the prior probability. A uniform distribution can be introduced if the prior probability is unavailable. Second, the likelihood of observing the ultimate load for a specific A can be estimated using a probabilistic prediction model, as suggested in a previous study by Lee et al. [31]. Finally, the posterior probability can be inferred using the Markov chain Monte Carlo (MCMC) method, which is utilized when the analytical calculation of the integral term in the denominator of Eq. (1) is infeasible [32]. In Section 2.1, the method for estimating the likelihood is described. The MCMC method for inferring the posterior probability is discussed in Section 2.2.

2.1. Estimation of the likelihood of observing the ultimate load (i.e., $p(F_u|A)$)

Strands consist of multiple steel wires that are vulnerable to corrosion. Hence, the effects of corrosion on the structural capacity of prestressing strands have been widely studied. Recently, Lee et al. [31] proposed a method to probabilistically estimate the ultimate tensile strength of prestressing strands with pit corrosion. The method consists of four parts: (a) physics-based structural analysis modeling, (b) nonparametric surrogate model construction, (c) random sample generation using a constructed surrogate model, and (d) goodness-of-fit test. The method is briefly described in this study. The details can be found in Lee et al. [31].

The structural analysis modeling was divided into two steps. First, FE modeling was performed for the steel wires, which are components of strands. Second, theoretical modeling was conducted for the prestressing strands based on the FE analysis results. This is considered practical because the FE modeling of complex geometries and interactions between wires (i.e., one core wire with twisted helical wires around it) can be avoided [31]. Costello [33] developed a model based on a thin-rod theory to consider the effects of geometrical properties and interactions between wires. The ultimate load of each corroded wire can be derived from the FE model, which is then used to estimate the ultimate load of the prestressing strands based on Costello's model. In steel wires, pit corrosion can exist in several shapes and must be carefully designed in the FE model; here, hemisphere-shaped pits were considered in this study. Furthermore, the corroded sectional area at the most corroded section along the strands was considered as a significant factor affecting the mechanical properties of the strands for model simplification, the reason for which is discussed in Section 3.

The structural analysis model may be computationally expensive; therefore, the construction of a surrogate model can be considered to reduce the computational cost. The surrogate model is a numerical function that approximates the specified structural analysis model and can be constructed in two steps: design of experiments (DoE) and mapping (i.e., regression). DoE is a process for designing the experimental data to be used for mapping. Lee et al. [31] employed the central composite design (CCD) method proposed by Myers et al. [34]. Once the experimental data were collected from the FE models using the CCD method, mapping was performed. Among the various mapping techniques, kriging, which is a machine learning-based non-parametric regression, can be used to efficiently construct a surrogate model [31].

The ultimate load of the prestressing strands can be generated using the computationally efficient surrogate model. The model inputs that can affect the ultimate load are the corroded sectional area, material properties of steel (e.g., ultimate strength and strain), and size of the wires (e.g., diameters of the core and helical wires). As these inputs possess uncertainties, the resultant ultimate load also has a probabilistic property. Therefore, by determining the effects of the probabilistic properties of the input variables on the output variable, the conditional

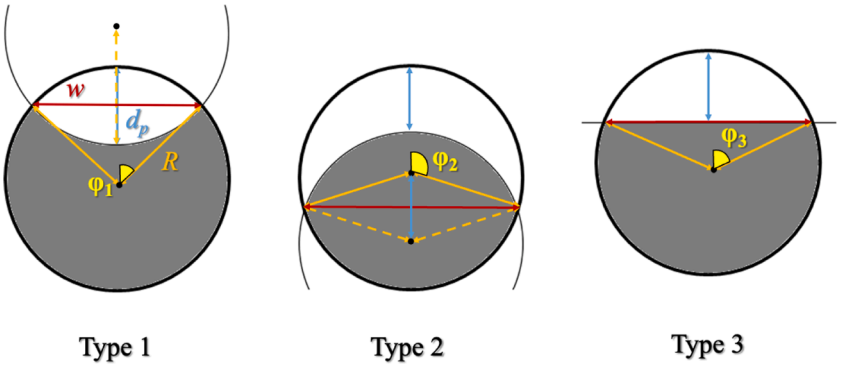


Fig. 1. Three types of sectional shapes of pit corrosion.

probability $p(F_u|A)$ in Eq. (3) can be derived. Monte Carlo sampling and a goodness-of-fit test are introduced to identify the best-fit probability distribution and probabilistic properties (e.g., mean and standard deviation). Monte Carlo sampling [35] is used to generate random samples for each random input. The resultant ultimate load is derived by incorporating these inputs into the constructed surrogate model. Goodness-of-fit tests, such as the Anderson–Darling test, can be utilized to determine the best-fit distribution for the generated samples of ultimate loads [35]. Consequently, a probability density function (PDF) for the ultimate loads for a certain sectional area at the most corroded section (i.e., $p(F_u|A)$) can be derived, which means that the likelihood of observing a certain ultimate load can be estimated as the probability density.

2.2. Estimation of the posterior probability: Markov chain Monte Carlo algorithm

As shown in Eq. (1), the posterior probability is the product of the likelihood and prior probability divided by an integral term, which is often called a normalizing factor because it creates the integral of the posterior probability distribution along the entire range. However, in several cases, estimating the normalizing factor is computationally expensive or infeasible. Thus, the MCMC method can be used to estimate it efficiently. MCMC is an iterative sampling method based on the Markov property, in which the conditional probability of observing a certain event depends only on the states of the previous event [36]. Because the conditional probability of observing the ultimate loads is determined by the sectional area (i.e., likelihood), MCMC can be employed to iteratively generate samples. There are two widely used MCMC methods: the MH algorithm [37] and Gibbs sampling [38]. The MH algorithm is used in this study.

The conditional probability of the sectional area for a specific ultimate load (i.e., $p(A|F_u)$), which is the posterior probability under the present condition, is proportional to the product of $p(F_u|A)$ and $p(A)$, as expressed in Eq. (3). The first step is to infer the $p(A|F_u)$ using the MH algorithm from the starting point A_0. In general, the MH algorithm leads to the convergence of the stationary condition regardless of the location of the starting point [36]. However, to enhance the computational efficiency, the starting point can be determined through the following optimization problem:

$$A_0 = \underset{A}{argmax}\, p(F_u|A)p(A) \tag{4}$$

Note that if we do not have any prior information about A, then the optimization process can be replaced by determining the mode of $p(F_u|A)$. From this initialization, the sampling period for converging to the stationary condition, the so-called burn-in period, can be significantly reduced, which prevents wasting of samples. This yields computational savings by avoiding unnecessary iterations during the burn-in period. Then, we can obtain $p(F_u|A_0)p(A_0)$. The $(t+1)$th point is generally determined in terms of the previous point (A_t, which is the tth point) by $A_* = A_t + \delta_*$, where δ_* follows a multivariate normal distribution with zero mean, and the standard variation is controlled empirically. When there is prior knowledge of the maximum or minimum values of the inferred value (i.e., A), a truncated normal distribution can be introduced. For example, because the maximum sectional area of non-corroded strands is known in our example, the maximum inference

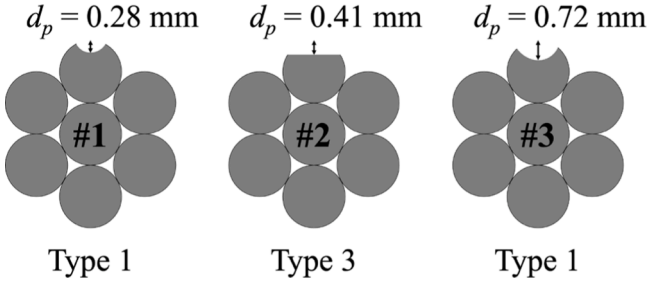


Fig. 2. Illustrations of the most corroded section of the three specimens.

Table 1
Corrosion configurations and tensile test results of three specimens of corroded strands.

Specimen	Corrosion type	Pit depth (mm)	Ultimate load (kN)
A	1	0.280	205.653
B	3	0.410	261.504
C	1	0.720	237.794

Table 2
Comparison of optimization and experimental results from tensile tests.

Specimen		Corrosion type	Pit depth (mm)	Corroded sectional area (mm^2)
A	Optima	1	0.2804	0.3104
		2	0.0837	0.3139
		3	0.2237	0.3112
	Experimental Value	1	0.2800	0.3097
B	Optima	1	0.5137	0.7641
		2	0.2059	0.7721
		3	0.4132	0.7720
	Experimental Value	3	0.4100	0.7632
C	Optima	1	0.7248	1.2982
		2	0.3402	1.2754
		3	0.5912	1.3061
	Experimental Value	1	0.7200	1.2598

Table 3
Ultimate load and sectional area at the most corroded section for each specimen.

Specimen #	Actual ultimate load (kN)	Actual sectional area (mm^2)	Specimen	Actual ultimate load (kN)	Actual sectional area (mm^2)
1	223.69	137.78	53	158.75	118.08
2	264.12	137.20	54	172.43	124.49
3	251.94	138.31	55	132.52	111.59
4	223.10	138.24	56	134.18	125.57
5	184.14	138.54	57	146.14	115.97
6	240.65	136.04	58	147.92	123.52
7	204.44	137.35	59	134.38	118.88
8	228.12	137.99	60	131.25	111.39
9	236.66	133.41	61	124.69	95.33
10	212.61	136.24	62	179.22	130.00
11	226.70	137.14	63	174.68	127.29
12	170.29	138.25	64	177.65	130.80
13	194.69	138.11	65	171.62	135.23
14	143.12	137.54	66	166.33	120.47
15	223.69	137.47	67	171.61	130.45
16	264.12	137.90	68	173.16	125.79
17	251.94	135.88	69	173.59	129.88
18	223.10	137.18	70	180.99	126.46
19	184.14	132.62	71	172.18	132.48
20	240.65	135.74	72	173.68	123.96
21	204.44	134.24	73	170.51	118.88
22	228.12	138.72	74	151.90	107.48
23	236.66	138.06	75	184.00	118.40
24	212.61	136.96	76	175.60	132.95
25	226.70	134.70	77	186.40	127.01
26	170.29	137.49	78	168.60	129.58
27	194.69	137.17	79	177.85	131.41
28	143.12	137.75	80	170.34	124.71
29	223.69	137.99	81	173.38	128.04
30	264.12	136.75	82	150.17	132.01
31	251.94	138.72	83	145.11	135.11
32	223.10	138.72	84	128.29	137.82
33	184.14	138.72	85	171.17	137.50
34	240.65	138.72	86	138.46	136.57
35	204.44	138.72	87	183.83	134.45
36	228.12	138.22	88	184.98	118.65
37	236.66	131.20	89	184.03	136.64
38	212.61	132.90	90	223.69	131.88
39	226.70	136.11	91	264.12	136.71
40	170.29	134.14	92	251.94	121.03
41	194.69	135.99	93	223.10	133.05
42	143.12	136.89	94	184.14	133.17
43	223.69	131.56	95	240.65	130.74
44	264.12	130.16	96	204.44	121.52
45	251.94	138.72	97	228.12	111.30
46	223.10	133.77	98	236.66	118.65
47	184.14	137.56	99	212.61	133.98
48	240.65	126.33	100	226.70	132.19
49	204.44	131.98	101	170.29	138.72
50	228.12	131.85	102	194.69	138.72
51	236.66	128.26	103	143.12	138.72
52	212.61	125.27	-	–	–

Table 4
Statistical properties of the random variables considered in the wire model.

Random variables	Mean	Coefficient of variation	Probability distribution
Ultimate Strength of Steel	1865 MPa	0.02	Normal
Ultimate Strain of Steel	0.075	0.08	Normal
Diameter of Core Wire	5.16 mm	0.012	Normal
Diameter of Helical Wire	5.00 mm	0.012	Normal
Sectional Loss Area (***sla***)	*sla*	*sla* ·0.05	Lognormal

value of the sectional area was limited by introducing a truncated normal distribution. Accordingly, we can also obtain $p(F_u|A_*)p(A_*)$, and the acceptance probability (α) is calculated as follows:

$$\alpha = min\left(1, \frac{p(F_u|A_*)p(A_*)}{p(F_u|A_t)p(A_t)}\right) \tag{5}$$

When a random number generated from a uniform distribution is less than the acceptance probability, a new point is accepted (i.e., $A_{t+1} = A_*$); otherwise, the previous sample is considered (i.e., $A_{t+1} = A_t$). By iteratively generating samples using this procedure, the stationary distribution of a sectional area at the most corroded section can be inferred.

3. Parametric study: Modeling of pit corrosion

The pit corrosion of prestressing strands has an irregular hemispherical shape; therefore, constructing an exact model of every type of corrosion would be impractical. Various researchers have studied model simplification. Cerit et al. [28] introduced a hemispherical shape to design pit corrosion in an FE model. Li et al. [39] designed a pit corrosion model using anticlastic and spheroid shapes. Jeon et al. [40] concluded that the geometric properties of the most corroded section (e.g., the sectional shape of the corrosion, maximum pit depth, and pit width) can be considered to simplify the model of corroded wires. Three types of sectional shapes of pit corrosion were proposed, as shown in Fig. 1 [31,40].

Fig. 1 shows the corroded areas with white spaces, whereas the gray spaces denote the non-corroded sectional area, and the pit width, depth, and sectional radius are w, d_p, and R, respectively. The corrosion angle (φ_i, where $i = 1,\ldots, 3$) and sectional area ($A_{type,i}$, where $i = 1,\ldots, 3$) can be calculated using Eqs. (6)–(11) for $0 \le d_p \le 2R$.

$$\varphi_1 = arccos\left(1 - \frac{d_p}{2R}\right) \tag{6}$$

$$A_{type,1} = 2R^2(\varphi_1 - sin\varphi_1 cos\varphi_1) \tag{7}$$

$$\varphi_2 = arccos\left(-\frac{d_p}{2R}\right) \tag{8}$$

$$A_{type,2} = R^2(2\varphi_2 - \pi - 2sin\varphi_2 cos\varphi_2) \tag{9}$$

$$\varphi_3 = arccos\left(1 - \frac{d_p}{R}\right) \tag{10}$$

$$A_{type,3} = R^2(\varphi_3 - sin\varphi_3 cos\varphi_3) \tag{11}$$

We revisited the assumption that the geometric properties of the most corroded section are important, as suggested by Jeon et al. (2019) [40], and particularly tested how the corrosion shapes affect the mechanical properties of strand specimens. Three 100 mm-long specimens of the seven-wire strand (i.e., one core wire with six helical wires) with a nominal diameter of 15.2 mm were prepared, and tensile tests were performed using a displacement control method at a speed of 5 mm/min until one wire fails. In these specimens, only on of the seven wires was corroded, as shown in Fig. 2. The corrosion configurations and tensile test results are listed in Table 1. Structural analysis models were constructed based on the studies by Jeon et al. [40] and Lee et al. [31], as described in Section 2.1.

The mechanical properties (e.g., ultimate load) of specific corrosion configurations and the conditional probability of observing the ultimate load can be estimated using the structural analysis model [31,40]. In this parametric study, we inversely inferred the corrosion configurations for specified mechanical properties. The aim was to determine the optimal corrosion configurations of a model that accurately estimated the actual mechanical properties of the given specimens. Therefore, an optimization problem was designed as follows:

Table 5
Accuracy of the surrogate-based prediction model for estimating ultimate loads of strands.

Scenario	Random variables					Ultimate load from FE model (kN)	Prediction result of surrogate model (kN)	Absolute error (%)
	Ultimate strength (MPa)	Ultimate strain	Diameter of core wire (mm)	Diameter of helical wires (mm)	Sectional loss area (mm^2)			
1	1851.11	0.085	5.20	5.07	0.45	261.64	260.13	0.58
2	1848.08	0.076	5.14	5.01	2.33	248.83	245.77	1.23
3	1881.20	0.075	5.12	4.91	24.39	167.81	160.23	4.52
4	1861.90	0.069	5.18	5.02	3.55	246.60	244.03	1.04
5	1848.33	0.071	5.13	5.05	0.00	258.41	259.03	0.24
6	1875.68	0.063	5.21	5.04	13.82	213.28	207.38	2.76
7	1875.83	0.079	5.20	5.00	0.00	258.93	257.77	0.45
8	1857.98	0.065	5.16	4.88	1.21	243.55	245.53	0.81
9	1856.40	0.074	5.13	4.94	4.88	233.08	230.10	1.28
10	1840.62	0.076	5.16	4.90	0.00	244.93	244.25	0.28
Arithmetic Mean of Absolute Error (%)								1.32

$$\left[\widehat{d_{pit}}, \widehat{t_{pit}}\right] = \underset{d_{pit}, t_{pit}}{\operatorname{argmax}}\, p\left(F_u \middle| d_{pit}, t_{pit}\right) \tag{12}$$

where F_u represents the ultimate load obtained from the tensile test, and $p(F_u|d_{pit}, t_{pit})$ is the conditional probability of observing the ultimate load with a pit depth of d_{pit} and corrosion type (i.e., shape) of t_{pit}. Consequently, the pit depth and corrosion type that maximized the likelihood (i.e., $\widehat{d_{pit}}$ and $\widehat{t_{pit}}$) were inferred as the optimal corrosion configurations.

Table 2 lists the optimization results for the specimens. There are three optima for each corrosion type. For instance, Specimen A has three optima for the corrosion type and pit depths of 1 and 0.2804; 2 and 0.0837; and 3 and 0.2237. The optimized pit depth agreed with the experimental results for the equivalent corrosion type. This indicates that the structural analysis model based on the corrosion configurations of the most corroded section is applicable to the actual problem. In addition, the optimization results showed that the corroded sectional areas of the three optima were close to the experimental values regardless of the corrosion type. For instance, the corroded sectional areas of the three optima for Specimens A, B, and C are approximately 0.31, 0.77, and 1.26 mm^2, respectively, regardless of the corrosion type. Here, we concluded that the structural analysis model, which was constructed based on Jeon et al. [40] and Lee et al. [31], could be simplified without considering the corrosion type; and the corroded sectional area should be considered as the dominant input of the model. From this finding, the corroded sectional area at the most corroded section along strands is considered a dominant factor affecting the mechanical properties of strands in this study, for the purpose of problem simplification.

4. Applications

4.1. Example 1: Probabilistic inference using tensile test results of strands

The proposed method was applied to infer the corrosion of strands with multiple prestressing wires. A total of 103 corroded seven-wire strands (Specimens 1–103) with a length of 100 mm were collected from a bridge in South Korea. The nominal diameters were 15.2 mm for Specimens 1–61 and 12.7 mm for Specimens 62–103. The sectional area at the most corroded section was estimated by repeatedly measuring the pit depth using a pit depth gauge. After measuring the corrosion, tensile tests were conducted using the displacement control method at a speed of 5 mm/min until any wire failed. The ultimate loads and sectional areas at the most corroded sections are listed in Table 3. The sectional area (i.e., the original area minus the corroded area), rather than the corroded sectional area, was recorded to account for the uncertainty present in the original sectional area without corrosion.

FE analysis models for the prestressing wires were constructed using the commercial software ABAQUS. The corrosion shape was designed as Type 1, as suggested by Jeon et al. [40]. As proposed by Lee et al. [31], the statistical properties of the five random variables listed in Table 4 were considered, and a surrogate model was constructed using CCD and kriging methods. Costello's model was employed to consider the effects of the geometrical properties and interactions between prestressing wires, and a prediction model for estimating the ultimate load for a given sectional area was derived. Table 5 lists the prediction accuracy of the surrogate model compared with the FE analysis results for various combinations of random variables. The results show an average absolute error of approximately 1%. Notably, the surrogate model has a significant advantage in terms of the computational time, with each computation completed in less than 0.1 s, whereas the FE model requires approximately 30 min (i.e., 1800 s) on a regular personal computer. The significant reduction in computational cost further supports the practical applicability of the constructed surrogate model. Monte Carlo sampling, based on the derived prediction model with consideration of the probabilistic properties of the five random variables in Table 4 and the Anderson–Darling test, showed that the ultimate load of the prestressing strands was well fitted by two parametric (i.e., k and λ) Weibull distributions, where the PDF was defined as follows:

$$F_u \sim f_{weibull}(A) = \frac{k}{\lambda}\left(\frac{A}{\lambda}\right)^{k-1} e^{-(A/\lambda)^k} \tag{13}$$

This indicates that the likelihood of observing a certain ultimate load for a specific A (i.e., $p(F_u|A)$) can be estimated as the PDF of the Weibull distribution.

A total of 250 000 random samples for A were generated using the MH algorithm. It was assumed that the maximum area of a non-corroded strand was a 95% upper value, considering the statistical properties of the diameters in Table 4, which is 145.32 mm^2. That is, we truncated the resulting PDFs at 145.32 mm^2, which ensured that the inference remained within the range of realistic values. In addition, a uniform distribution was assumed for $p(A)$ owing to the absence of prior information on the sectional area. The probabilistic inference results in Fig. 3 (probability density plots and quantitative values can be found in Appendix A and Appendix B, respectively) show the 50% and 95% inference bounds and experimental values of each specimen. For example, the experimental value of Specimen 26 was within its 95% inference bound but out of the 50% bound, whereas the actual sectional area of Specimen 25 was within both the 50% and 95% inference bounds. As summarized in Table 6, the number of specimens whose actual value was within the 50% and 95% inference bounds was 62 (i.e., 60.19% of the 103 specimens) and 90 (i.e., 87.38% of the 103 specimens), respectively.

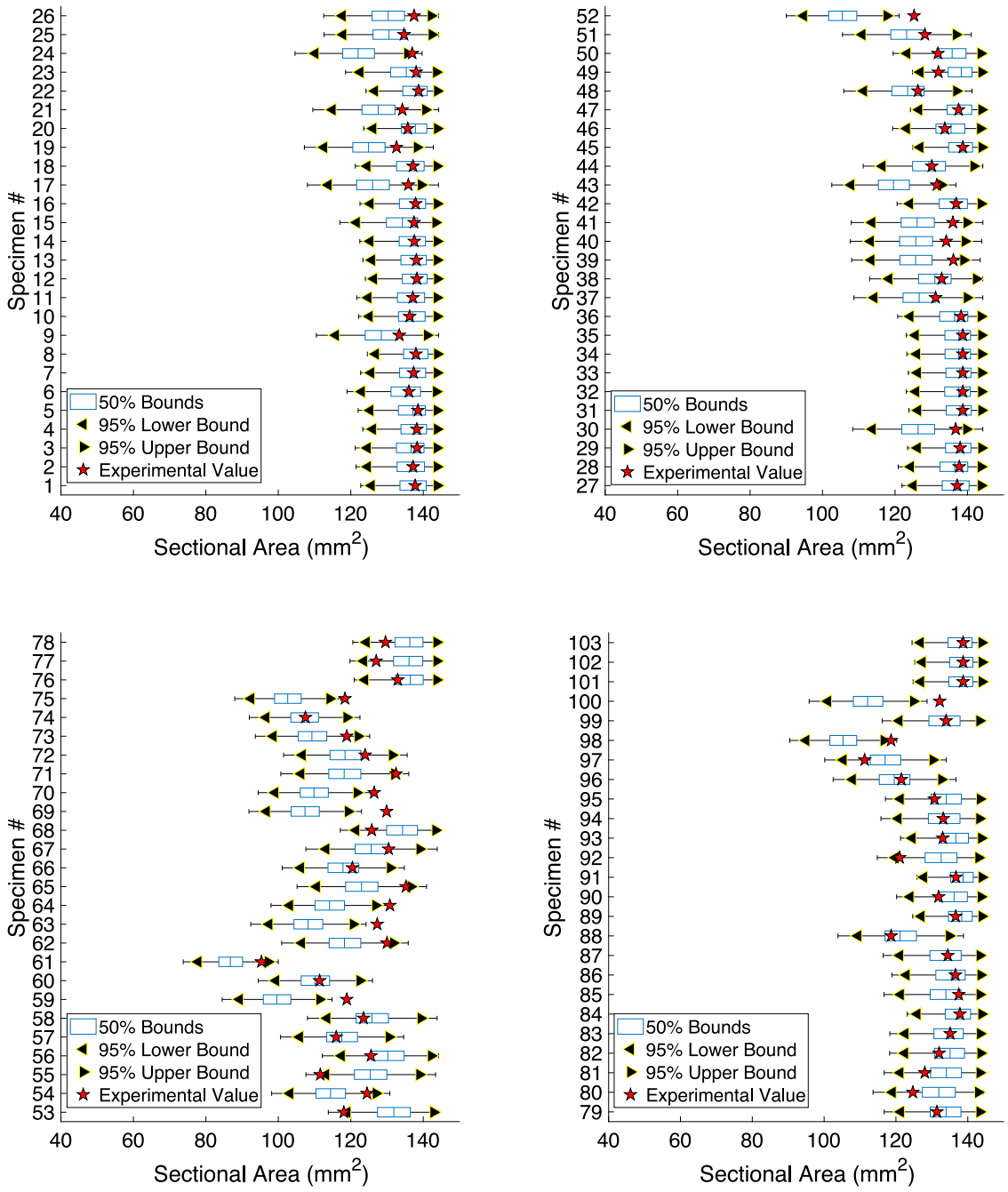


Fig. 3. Inference results and experimental sectional areas at the most corroded section for each specimen.

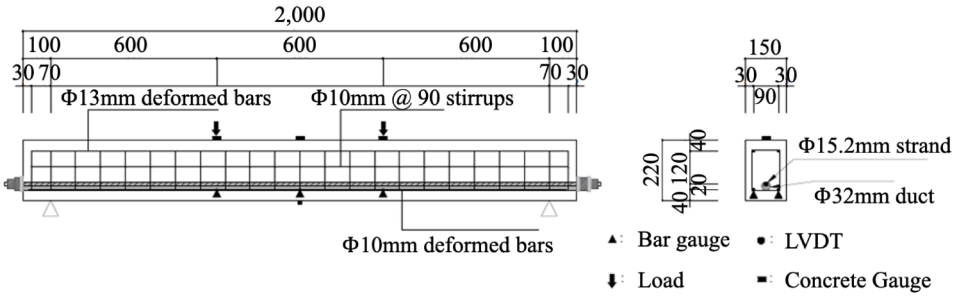
Table 6
Inference and experimental results for the twelve specimens.

Among 103 specimens	Within 50% bounds	Within 95% bounds
Number	62	90
Ratio	60.19%	87.38%

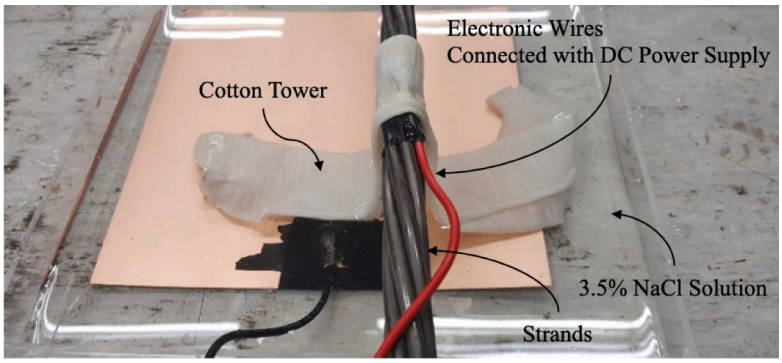
4.2. *Example 2: Probabilistic inference using bending test results of girders*

The proposed method was further applied to infer the corrosion of embedded strands in PSC girders. In Section 4.1, the ultimate loads of the corroded strands were directly specified so that the corrosion could be inferred using the proposed method. In this section, a situation is considered in which the ultimate load of the strand embedded in the PSC girder is unknown, but a validated FE model for the PSC girder is available. Thus, the first step is to infer the ultimate load of the embedded strands from the FE models for PSC girders. Then, the corrosion of the strand is inferred based on the inferred ultimate load, as described in Section 4.1.

Three PSC girder specimens (G1–G3) were prepared according to the design shown in Fig. 4(a) [41]. The compressive strength and elastic modulus of the non-corroded concrete containing a corroded strand were 43.85 and 36076.55 MPa, respectively. The corrosion of the pre-stressing strand at the center of the strands was first induced by continuously passing an electric current through the area exposed to NaCl using a cotton towel (Fig. 4(b)). Then, the concrete was cast (i.e., no concrete cracking or spalling occurred). The sectional area at the

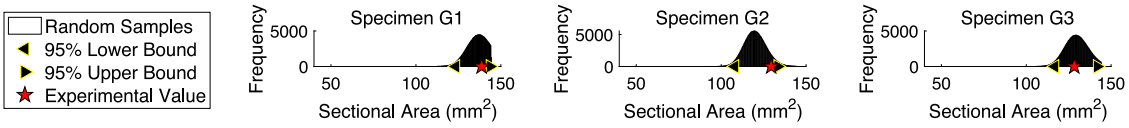


(a)

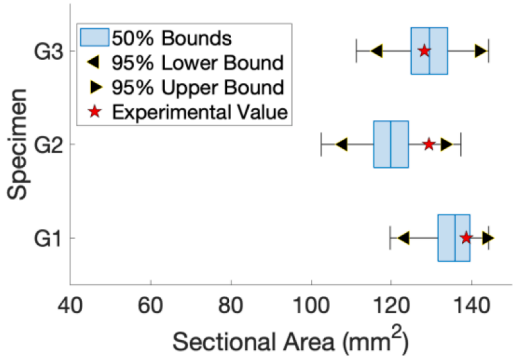


(b)

Fig. 4. (a) Design of the specimens and (b) electrochemical corrosion-inducing method.



(a)



(b)

Fig. 5. Inference results and experimental sectional areas at the most corroded section: (a) probability density function plots and (b) box plots.

Table 7
Ultimate loads of the PSC girders obtained from the four-point bending test.

Specimen	Ultimate load of the girder (kN)
G1	151.50
G2	135.20
G3	149.38

Table 8
Optimal ultimate loads and actual sectional areas of the embedded strands.

Specimen	Optimal ultimate load of embedded strand (kN)	Actual sectional area of embedded strand (mm^2)
G1	252.3	138.67
G2	215.7	129.42
G3	236.4	128.28

Table 9
Inference and experimental results for the two specimens ("X" indicates that the value is located out of bounds, whereas "O" means that the value is within the bounds, indicating a successful inference).

Specimen	Inference results				Experimental value	Within the 50% bounds?	Within the 95% bounds?
	50% Lower bound	50% Upper bound	95% Lower bound	95% Upper bound			
G1	131.64	139.63	123.45	143.69	138.67	O	O
G2	115.57	124.27	107.96	133.35	129.42	X	O
G3	124.94	134.06	116.77	141.85	128.28	O	O

most corroded section of the strand was measured using the pit depths before concrete casting (Table 7 [41]). The width, height, and span of the concrete part were 150, 220, and 2000 mm, respectively, and the nominal value of the sectional area of the non-corroded strand was 138.7 mm^2. A four-point bending test was conducted until either the compressive strain of the concrete exceeded 0.003 or at least one wire failed. The vertical deflection was measured using a linear variable differential transformer sensor at the midspan. The resultant ultimate loads of the PSC girders ($F_{u,girder}$) are summarized in Table 7 [41].

The FE model validated by Jeon et al. [41] was used. It was prepared using ABAQUS, and the concrete and strands were designed as two-dimensional plane and truss elements, respectively. Imperfect bonding between the strand and concrete was assumed due to corrosion, and was modeled as de-bonded. The nonlinearity of concrete was considered using a concrete damage plasticity model in ABAQUS.

$$\frac{\sigma_c}{f_{cc}} = \frac{\left(1.05 \times E_c \times {}^{0.0238}/_{f_{cc}}\right) \times \varepsilon_c/0.0238 - \left(\varepsilon_c/0.0238\right)^2}{1 + \left(\left(1.05 \times E_c \times {}^{0.0238}/_{f_{cc}}\right) - 2\right) \times \varepsilon_c/0.0238} \tag{14}$$

where σ_c and ε_c are the stress and strain of concrete, respectively. The bending test results of the PSC girder are available, whereas the ultimate load of the embedded strand is unknown. Therefore, the optimization problem for determining the optimal ultimate load of the strand ($\widehat{F_u}$) is introduced as follows:

$$\widehat{F_u} = \underset{F_u}{\operatorname{argmin}} \left(F_{u,girder} - F_{model}(F_u)\right)^2 \tag{15}$$

where $F_{model}(F_u)$ denotes the ultimate load of the PSC girder with input of F_u (i.e., the ultimate load of the strand) obtained from the validated FE model. We introduced a simplified but validated two-dimensional FE model to reduce the optimization cost and employed the optimization function *fmincon*, which is a built-in MATLAB function that performs constrained nonlinear optimization. The optimal ultimate loads of the embedded strands are listed in Table 8. These were used to infer the sectional areas at the most corroded sections of the strands using the proposed method, which are summarized in Table 8.

A total of 250 000 random samples for the A_{corr} were generated using the MH algorithm. It was assumed that the maximum area is a 95% upper value considering the statistical properties of the diameters in Table 4, which is 145.32 mm^2, and a uniform distribution was assumed for $p(A)$ because of the absence of a prior guess. The PDFs and box plots for each specimen are shown in Fig. 5(a) and (b), respectively. As summarized in Table 9, the experimental values of each specimen lie within the 95% inference bound, and two of them are located within the 50% inference bound. This indicates that the proposed method can be used to infer the corrosion of embedded strands in PSC girders using the validated FE models.

5. Conclusions

In this study, a Bayesian inference method was proposed to indirectly monitor pit corrosion in the prestressing strands of PSC bridges. This is an inverse analysis method that uses computer simulation models. First, a parametric study to simplify corrosion modeling was conducted. It was concluded that the pit corrosion of the strands could be represented by the sectional area at the most corroded section. Subsequently, the conditional probabilities between the ultimate load of the strands and sectional area at the most corroded section were defined in terms of Bayes' rule based on a preliminary study conducted by Lee et al. (2020). Finally, the MCMC method for estimating the posterior probability was introduced, which is the conditional probability of the sectional area given a certain ultimate load. Probabilistic inference bounds were derived based on the samples generated using MCMC.

Two case studies were conducted using the proposed method. First, the probabilistic corrosion inference of the 103 strand specimens based on the tensile test results was performed. The 50% and 95% probabilistic inference bounds were derived using the proposed method, and the inference results showed good agreement with the actual values. The number of specimens with actual values within the 50% and 95% inference bounds were 62 (60.19% of 103 specimens) and 90 (87.38% of 103 specimens), respectively. Furthermore, the proposed method was applied to the problem of inferring the corrosion of the embedded strand in three PSC girder specimens. In this case, the ultimate load of the corroded strands was not provided directly and had to be estimated. Therefore, the ultimate load of the embedded strand was estimated by solving the optimization problem using the validated FE model, and then the corrosion was inferred. The resultant inference results showed good agreement with the experimental values; the experimental values of each specimen were within the 95% bound, and two of them were within the 50% inference bound. Based on these findings, we conclude that the proposed method can be used to predict the corrosion of embedded strands in PSC girders using verified FE models. The application was limited to single-strand problems. Thus, we expect that the proposed method will be further studied to solve the problem of inferring the corrosion of embedded tendons comprising multiple strands.

Declaration of competing interest

The authors declare that they have no known competing financial interests or personal relationships that could have appeared to influence the work reported in this paper.

Data availability

Data will be made available on request

Acknowledgments

This work was supported by the National Research Foundation of Korea (NRF) grant funded by the Korea government (MSIT [2021R1C1C2008770]).

Appendix A. Density plots of specimens #1 to 103




Specimen #52
Specimen #53
Specimen #54
Specimen #55
Specimen #56
Specimen #57
Specimen #58
Specimen #59
Specimen #60
Specimen #61
Specimen #62
Specimen #63
Specimen #64
Specimen #65
Specimen #66
Specimen #67
Specimen #68
Specimen #69
Specimen #70
Specimen #71
Specimen #72
Specimen #73
Specimen #74
Specimen #75
Specimen #76
Specimen #77
Specimen #78
Specimen #79
Specimen #80
Specimen #81
Specimen #82
Specimen #83
Specimen #84
Specimen #85
Specimen #86
Specimen #87
Specimen #88
Specimen #89
Specimen #90
Specimen #91
Specimen #92
Specimen #93
Specimen #94
Specimen #95
Specimen #96
Specimen #97
Specimen #98
Specimen #99
Specimen #100
Specimen #101
Specimen #102
Specimen #103
Frequency
Sectional Area (mm2)

Appendix B. Quantitative values of inference results for specimens #1 to 103

See Table B.1

Table B.1
Quantitative values of inference results for specimens #1 to 103.

Specimen #	50% Lower bound	50% Upper bound	95% Lower bound	95% Upper bound	Experimental value	Within the 50% bounds?	Within the 95% bounds?
1	133.58	140.81	125.69	143.87	137.78	O	O
2	132.79	140.34	124.64	143.81	137.20	O	O
3	132.61	140.21	124.56	143.79	138.31	O	O
4	133.86	140.90	126.03	143.89	138.24	O	O
5	133.16	140.57	125.32	143.82	138.54	O	O
6	131.12	139.23	122.98	143.59	136.04	O	O
7	133.49	140.68	125.55	143.85	137.35	O	O
8	134.59	141.27	126.86	143.93	137.99	O	O
9	123.99	132.99	115.82	141.12	133.41	X	O
10	133.19	140.52	125.13	143.83	136.24	O	O
11	132.88	140.38	124.77	143.82	137.14	O	O
12	134.24	141.05	126.35	143.91	138.25	O	O
13	133.84	140.85	125.78	143.86	138.11	O	O
14	133.37	140.62	125.34	143.84	137.54	O	O
15	129.85	138.44	121.57	143.46	137.47	O	O
16	133.42	140.66	125.39	143.87	137.90	O	O
17	121.60	130.65	113.78	139.45	135.88	X	O
18	132.65	140.25	124.51	143.80	137.18	O	O
19	120.55	129.46	112.59	138.33	132.62	X	O
20	134.01	140.99	126.13	143.89	135.74	O	O
21	123.09	132.17	114.91	140.65	134.24	X	O
22	134.35	141.12	126.62	143.92	138.72	O	O
23	130.98	139.27	122.56	143.64	138.06	O	O
24	117.76	126.54	110.17	135.66	136.96	X	X
25	126.14	135.16	117.83	142.43	134.70	O	O
26	125.89	134.83	117.68	142.20	137.49	X	O
27	133.04	140.45	125.05	143.81	137.17	O	O
28	132.42	140.10	124.31	143.76	137.75	O	O
29	133.98	140.98	126.18	143.91	137.99	O	O
30	121.89	130.93	113.78	139.76	136.75	X	O
31	134.17	141.05	126.32	143.91	138.72	O	O
32	133.73	140.80	125.79	143.87	138.72	O	O
33	134.06	140.98	126.21	143.89	138.72	O	O
34	133.81	140.85	126.02	143.89	138.72	O	O
35	133.77	140.87	125.63	143.89	138.72	O	O
36	132.35	140.09	124.18	143.76	138.22	O	O
37	122.23	131.28	114.25	139.92	131.20	O	O
38	126.50	135.50	118.33	142.43	132.90	O	O
39	121.35	130.22	113.39	138.96	136.11	X	O
40	121.28	130.35	113.23	139.31	134.14	X	O
41	121.69	130.86	113.64	139.86	135.99	X	O
42	132.22	139.98	124.07	143.76	136.89	O	O
43	115.41	123.97	107.86	132.81	131.56	X	O
44	124.84	133.92	116.50	141.76	130.16	O	O
45	134.80	141.40	126.91	143.97	138.72	O	O
46	131.30	139.28	123.21	143.59	133.77	O	O
47	134.39	141.16	126.60	143.93	137.56	O	O
48	119.14	127.99	111.38	136.99	126.33	O	O
49	134.69	141.26	126.94	143.94	131.98	X	O
50	131.55	139.61	123.31	143.70	131.85	O	O
51	118.83	127.72	110.93	136.89	128.26	X	O
52	101.67	109.46	94.79	117.79	125.27	X	X
53	127.39	136.45	119.00	142.89	118.08	X	X
54	110.38	118.54	103.19	127.00	124.49	X	O
55	121.02	129.98	113.14	139.00	111.59	X	X
56	125.69	134.73	117.43	142.24	125.57	X	O
57	113.35	121.85	105.88	130.60	115.97	O	O
58	121.46	130.41	113.44	139.36	123.52	O	O
59	95.87	103.45	89.29	111.40	118.88	X	X
60	106.30	114.17	99.32	122.53	111.39	O	O
61	83.57	90.14	77.85	97.22	95.33	X	O
62	114.02	122.77	106.46	131.77	130.00	X	O
63	104.32	112.28	97.44	120.66	127.29	X	X
64	110.13	118.25	103.15	126.86	130.80	X	X
65	118.58	127.52	110.55	136.62	135.23	X	O
66	113.71	122.14	106.17	130.91	120.47	O	O
67	121.20	130.27	113.16	139.06	130.45	X	O

(continued on next page)

Table B.1 (*continued*)

Specimen #	50% Lower bound	50% Upper bound	95% Lower bound	95% Upper bound	Experimental value	Within the 50% bounds?	Within the 95% bounds?
68	129.89	138.42	121.44	143.44	125.79	X	O
69	103.54	111.32	96.74	119.31	129.88	X	X
70	106.06	113.81	99.10	121.70	126.46	X	X
71	113.92	122.77	106.26	132.10	132.48	X	X
72	114.25	122.79	106.63	131.45	123.96	X	O
73	105.49	113.38	98.59	122.04	118.88	X	O
74	103.45	111.08	96.62	118.89	107.48	O	O
75	98.96	106.30	92.43	114.20	118.40	X	X
76	132.38	140.00	123.90	143.72	132.95	O	O
77	131.83	139.87	123.58	143.75	127.01	X	O
78	132.19	139.94	124.30	143.72	129.58	X	O
79	129.56	138.11	121.32	143.35	131.41	O	O
80	127.36	136.52	119.02	142.95	124.71	X	O
81	129.65	138.26	121.17	143.36	128.04	X	O
82	130.74	139.08	122.45	143.60	132.01	O	O
83	130.57	138.75	122.54	143.49	135.11	O	O
84	133.74	140.80	125.90	143.88	137.82	O	O
85	129.54	138.11	121.28	143.38	137.50	O	O
86	131.11	139.27	122.90	143.61	136.57	O	O
87	129.47	138.16	121.08	143.38	134.45	O	O
88	116.96	125.70	109.40	134.87	118.65	O	O
89	134.61	141.24	127.04	143.94	136.64	O	O
90	132.00	139.88	123.95	143.71	131.88	X	O
91	135.26	141.53	127.75	143.98	136.71	O	O
92	128.12	137.00	119.84	143.05	121.03	X	O
93	132.62	140.18	124.52	143.79	133.05	O	O
94	129.03	137.84	120.64	143.30	133.17	O	O
95	129.77	138.24	121.24	143.43	130.74	O	O
96	115.35	123.90	107.90	132.69	121.52	O	O
97	112.86	121.33	105.35	130.29	111.30	X	O
98	101.61	109.06	94.97	116.64	118.65	X	X
99	129.17	137.86	120.92	143.31	133.98	O	O
100	108.15	116.36	101.02	124.87	132.19	X	X
101	134.75	141.39	126.92	143.95	138.72	O	O
102	134.96	141.44	127.35	143.96	138.72	O	O
103	134.52	141.21	126.83	143.92	138.72	O	O

References

[1] A. Azizinamini, J. Gull, Improved Inspection Techniques for Steel Prestressing/post-Tensioning Strand: Vol. I, 2012.

[2] Y. Sun, Y. Kang, Magnetic mechanisms of magnetic flux leakage nondestructive testing, Appl. Phys. Lett. 103 (2013), 184104, https://doi.org/10.1063/1.4828556.

[3] H. Dunegan, D. Harris, Acoustic emission-a new nondestructive testing tool, Ultrasonics 7 (1969) 160–166, https://doi.org/10.1016/0041-624X(69)90660-X.

[4] N.J. Carino, The impact-echo method: an overview, in: Structures 2001: A Structural Engineering Odyssey, 2001, pp. 1–18, https://doi.org/10.1061/40558(2001)15.

[5] S. Huang, S. Wang, New Technologies in Electromagnetic Non-Destructive Testing, Springer, Singapore, 2016, https://doi.org/10.1007/978-981-10-0578-7.

[6] H. Wang, A. Yajima, R.Y. Liang, H. Castaneda, A Bayesian model framework for calibrating ultrasonic in-line inspection data and estimating actual external corrosion depth in buried pipeline utilizing a clustering technique, Struct. Saf. 54 (2015) 19–31, https://doi.org/10.1016/j.strusafe.2015.01.003.

[7] G.C. Moran, Corrosion Monitoring in Industrial Plants Using Nondestructive Testing and Electrochemical Methods: A Symposium (No. 908), ASTM International, 1986, https://doi.org/10.1520/STP908-EB.

[8] K. Sepahvand, S. Marburg, Identification of composite uncertain material parameters from experimental modal data, Probab. Eng. Mech. 37 (2014) 148–153, https://doi.org/10.1016/j.probengmech.2014.06.008.

[9] J.T.P. Yao, H.G. Natke, Damage detection and reliability evaluation of existing structures, Struct. Saf. 15 (1994) 3–16, https://doi.org/10.1016/0167-4730(94)90049-3.

[10] E.S. Diaz, R. Adey, J. Buynham, Prediction of the condition of a structure subject to corrosion based on inverse analysis, WIT Trans. Model. Simul. 34 (2003).

[11] Y. Xin, C. Mourad, C. Jin, An iterative BEM for the inverse problem of detecting corrosion in a pipe, Num. Mat.-Engl. Ser. 14 (2005) 252.

[12] J.L.A. De Oliveira e Sousa, R. Gettu, Determining the tensile stress-crack opening curve of concrete by inverse analysis, J. Eng. Mech. 132 (2006) 141–148, https://doi.org/10.1061/(ASCE)0733-9399(2006)132:2(141).

[13] Q. Yan, X. Yan, X. Yang, L. Zhang, Research of optimization inverse analysis technique on corrosion identification of buried pipeline wall, in: ICPTT 2009: Advances and Experiences with Pipelines and Trenchless Technology for Water, Sewer, Gas, and Oil Applications, 2009, https://doi.org/10.1061/41073(361)171, 1624–30.

[14] K. Minagawa, K. Suga, M. Kikuchi, S. Aoki, An efficient inverse analysis considering observation error to detect corrosion in concrete structures containing multilayered rebar, Int. J. Mech. Mater. Des. 8 (2012) 81–87, https://doi.org/10.1007/s10999-012-9178-6.

[15] S. Fonna, S. Huzni, A.K. Ariffin, Boundary element inverse analysis for rebar corrosion detection: Study on the 2004 tsunami-affected structure in aceh, Case Stud. Constr. Mater. 8 (2018) 292–298, https://doi.org/10.1016/j.cscm.2018.02.008.

[16] Y. Honjo, L. Wen-Tsung, S. Sakajo, Application of akaike information criterion statistics to geotechnical inverse analysis: the extended Bayesian method, Struct. Saf. 14 (1994) 5–29, https://doi.org/10.1016/0167-4730(94)90004-3.

[17] N. Tada, T. Kitamura, R. Ohtani, Probabilistic inverse analysis for predicting the distribution of multiple internal defects, Eng. Fract. Mech. 52 (1995) 1015–1027, https://doi.org/10.1016/0013-7944(95)00087-C.

[18] E.M.R. Fairbairn, N.F.F. Ebecken, C.N.M. Paz, F.J. Ulm, Determination of probabilistic parameters of concrete: solving the inverse problem by using artificial neural networks, Comput. Struct. 78 (2000) 497–503, https://doi.org/10.1016/S0045-7949(00)00073-0.

[19] T. Xu, L. White, D. Hui, Y. Luo, Probabilistic inversion of a terrestrial ecosystem model: Analysis of uncertainty in parameter estimation and model prediction, Glob. Biogeochem. Cy 20 (2006), https://doi.org/10.1029/2005GB002468.

[20] Y. Tsompanakis, N.D. Lagaros, G.E. Stavroulakis, Soft computing techniques in parameter identification and probabilistic seismic analysis of structures, Adv. Eng. Softw. 39 (2008) 612–624, https://doi.org/10.1016/j.advengsoft.2007.06.004.

[21] L. Wang, J.H. Hwang, Z. Luo, C.H. Juang, J. Xiao, Probabilistic back analysis of slope failure–a case study in Taiwan, Comput. Geotech. 51 (2013) 12–23, https://doi.org/10.1016/j.compgeo.2013.01.008.

[22] M. Chiachio, J. Chiachio, G. Rus, J.L. Beck, Predicting fatigue damage in composites: A Bayesian framework, Struct. Saf. 51 (2014) 57–68, https://doi.org/10.1016/j.strusafe.2014.06.002.

[23] J.B. Nagel, B. Sudret, A unified framework for multilevel uncertainty quantification in Bayesian inverse problems, Probabilistic Eng. Mech. 43 (2016) 68–84, https://doi.org/10.1016/j.probengmech.2015.09.007.

[24] H. Zhao, Z. Ru, C. Zhu, Determination of the geomechanical parameters and associated uncertainties in hydraulic fracturing by hybrid probabilistic inverse analysis, Int. J. Geomech. 17 (2017), 04017115, https://doi.org/10.1061/(ASCE)GM.1943-5622.0001014.

[25] P. Davidson, A.M. Waas, Probabilistic defect analysis of fiber reinforced composites using kriging and support vector machine based surrogates, Compos. Struct. 195 (2018) 186–198, https://doi.org/10.1016/j.compstruct.2018.03.007.

[26] E. Adeli, B. Rosić, H.G. Matthies, S. Reinstädler, D. Dinkler, Comparison of Bayesian methods on parameter identification for a viscoplastic model with damage, Probabilistic Eng. Mech. 62 (2020), 103083, https://doi.org/10.1016/j.probengmech.2020.103083.

[27] A. Imam, B.A. Salami, T.A. Oyehan, Predicting the compressive strength of a quaternary blend concrete using Bayesian regularized neural network, J. Struct. Integrity Maint. 6 (4) (2021) 237–246, https://doi.org/10.1080/24705314.2021.1892572.
[28] M. Cerit, K. Genel, S. Eksi, Numerical investigation on stress concentration of corrosion pit, Eng. Fail. Anal. 16 (2009) 2467–2472, https://doi.org/10.1016/j.engfailanal.2009.04.004.
[29] A. Castel, D. Coronelli, N.A. Vu, R. François, Structural response of corroded, unbounded posttensioned beams, J. Struct. Eng. 137 (2011) 761–771.
[30] F. Li, X. Luo, K. Wang, Y. Ji, Pitting damage characteristics on prestressing steel strands by combined action of fatigue load and chloride corrosion, J. Bridge Eng. 22 (2017), 04017023, https://doi.org/10.1061/(ASCE)BE.1943-5592.0001057.
[31] J. Lee, Y.-J. Lee, C.-S. Shim, Probabilistic prediction of mechanical characteristics of corroded strands, Eng. Struct. 203 (2020), 109882, https://doi.org/10.1016/j.engstruct.2019.109882.
[32] J. Kruschke, Doing Bayesian Data Analysis: a Tutorial with R, JAGS, and Stan. Elsevier Inc., 2014.
[33] G.A. Costello, Theory of Wire Rope, Springer Science & Business Media, 1997, https://doi.org/10.1007/978-1-4684-0350-3.
[34] R.H. Myers, D.C. Montgomery, C.M. Anderson-Cook, Response Surface Methodology: Process and Product Optimization Using Designed Experiments, John Wiley & Sons, 2016.
[35] A.H.S. Ang, W.H. Tang, Probability Concepts in Engineering: Emphasis on Applications in Civil & Environmental Engineering, Wiley, New York, 2007.
[36] S.P. Brooks, Markov chain Monte Carlo method and its application, J. Stat. 47 (1998) 69–100, https://doi.org/10.1111/1467-9884.00117.
[37] N. Metropolis, A.W. Rosenbluth, M.N. Rosenbluth, A.H. Teller, E. Teller, Equation of state calculations by fast computing machines, J. Chem. Phys. 21 (1953) 1087–1092, https://doi.org/10.1063/1.1699114.
[38] S. Geman, D. Geman, Stochastic relaxation, gibbs distributions, and the Bayesian restoration of images, IEEE Trans. Pattern Anal. Mach. Intell. 6 (1984) 721–741, https://doi.org/10.1109/TPAMI.1984.4767596.
[39] F. Li, X. Luo, K. Wang, Y. Ji, Pitting damage characteristics on prestressing steel strands by combined action of fatigue load and chloride corrosion, J. Bridge Eng. 22 (2017), 04017023, https://doi.org/10.1061/(ASCE)BE.1943-5592.0001057.
[40] C.-H. Jeon, J.-B. Lee, S. Lon, C.-S. Shim, Equivalent material model of corroded prestressing steel strand, J. Mater. Res. Technol. 8 (2019) 2450–2460, https://doi.org/10.1016/j.jmrt.2019.02.010.
[41] C.-H. Jeon, C.D. Nhuyen, C.-S. Shim, Assessment of mechanical properties of corroded prestressing strands, Appl. Sci. 10 (2020) 4055, https://doi.org/10.3390/app10124055.